# The Annual Cycle of the Energy Budget. Part II: Meridional Structures and Poleward Transports

JOHN T. FASULLO AND KEVIN E. TRENBERTH

*National Center for Atmospheric Research,* Boulder, Colorado*

(Manuscript received 7 March 2007, in final form 1 October 2007)

ABSTRACT

Meridional structure and transports of energy in the atmosphere, ocean, and land are evaluated holistically for the mean and annual cycle zonal averages over the ocean, land, and global domains, with discussion and assessment of uncertainty. At the top of the atmosphere (TOA), adjusted radiances from the Earth Radiation Budget Experiment (ERBE) and Clouds and Earth's Radiant Energy System (CERES) are used along with estimates of energy storage and transport from two global reanalysis datasets for the atmosphere. Three ocean temperature datasets are used to assess changes in the ocean heat content ($O_E$) and their relationship to the net upward surface energy flux over ocean ($F_S^o$), which is derived from the residual of the TOA and atmospheric energy budgets. The surface flux over land is from a stand-alone simulation of the Community Land Model forced by observed fields.

In the extratropics, absorbed solar radiation (ASR) achieves a maximum in summer with peak values near the solstices. Outgoing longwave radiation (OLR) maxima also occur in summer but lag ASR by 1–2 months, consistent with temperature maxima over land. In the tropics, however, OLR relates to high cloud variations and peaks late in the dry monsoon season, while the OLR minima in summer coincide with deep convection in the monsoon trough at the height of the rainy season. Most of the difference between the TOA radiation and atmospheric energy storage tendency is made up by a large heat flux into the ocean in summer and out of the ocean in winter. In the Northern Hemisphere, the transport of energy from ocean to land regions is substantial in winter, and modest in summer. In the Southern Hemisphere extratropics, land − ocean differences play only a small role and the main energy transport by the atmosphere and ocean is poleward. There is reasonably good agreement between $F_S^o$ and observed changes in $O_E$, except for south of 40°S, where differences among several ocean datasets point to that region as the main source of errors in achieving an overall energy balance. The winter hemisphere atmospheric circulation is the dominant contributor to poleward energy transports outside of the tropics [6–7 PW (1 petawatt = $10^{15}$ W)], with summer transports being relatively weak (~3 PW)—slightly more in the Southern Hemisphere and slightly less in the Northern Hemisphere. Ocean transports outside of the tropics are found to be small (<2 PW) for all months. Strong cross-equatorial heat transports in the ocean of up to 5 PW exhibit a large annual cycle in phase with poleward atmospheric transports of the winter hemisphere.

## 1. Introduction

The meridional contrast in the distribution of net downward radiation ($R_T$) at the top of the atmosphere (TOA) is largely imposed by the sun–Earth orbital geometry and thus is a fundamental property of the climate system, although it also reflects the collective influences of the atmospheric and ocean circulations, and the distributions of water vapor, clouds, and the surface on the planetary energy budget. Fasullo and Trenberth (2008, hereafter FT08) provide an assessment of the global energy budgets at the TOA and the surface, for the global atmosphere, and ocean and land domains based on a synthesis of satellite retrievals, reanalysis fields, a land surface simulation, and ocean temperature estimates. FT08 constrain the TOA budget to match estimates of the global imbalance during recent periods of satellite coverage associated with changes in atmospheric composition and climate. In this paper, the meridional profiles of the zonal mean energy budget reported by FT08 and its annual cycle are documented,

* The National Center for Atmospheric Research is sponsored by the National Science Foundation.

*Corresponding author address:* Kevin Trenberth, NCAR, P.O. Box 3000, Boulder, CO 80307-3000.
E-mail: trenbert@ucar.edu

DOI: 10.1175/2007JCLI1936.1

allowing a more complete assessment of possible error sources and a more comprehensive description of the energy budget.

The goal is improved quantification of the energy budget relative to previous analyses, which should be possible owing in part to recent major advances in observations provided by satellite data and globally gridded reanalyses (Trenberth et al. 2001; Trenberth and Stepaniak 2003a,b). Previous studies have documented the variability associated with the annual cycle (Trenberth and Stepaniak 2003a, 2004), and for El Niño–Southern Oscillation (ENSO) and interannual variability (Trenberth et al. 2002; Trenberth and Stepaniak 2003a). Addressed here is quantification of the meridional structure of both the annual mean and the annual cycle of energy transport and storage, and the improvement of uncertainty estimates associated with deficiencies in the duration of observations and other shortcomings. Moreover, as the surface budget is related to independent measurements of integrated ocean heat content ($O_E$), the degree of closure, or lack thereof, is assessed and aids in identifying specific shortcomings in ocean temperature fields. In addition, new estimates of the roles of the atmosphere and ocean in the meridional transport of energy along with quantification of the uncertainty and seasonal variability are provided.

Estimates of the transports have evolved from the early studies of Oort and Vonder Haar (1976, hereafter OV76), who made use of early low-resolution satellite, radiosonde, and hydrographic observations to provide an initial estimate of the Northern Hemisphere energy fluxes and transports, to direct calculation using radiative transfer codes applied to satellite retrievals (Zhang and Rossow 1997). More recently, analyses of global atmospheric reanalysis fields and TOA retrievals (Trenberth and Solomon 1994; Trenberth and Caron 2001) have been used to infer the ocean transports, although Wunsch (2005) has approached the problem from an oceanographic perspective and improved the assessments of the error bars. Here, we attempt to make a comprehensive analysis of the mean and annual cycle of meridional energy transports by the ocean and atmosphere and uncertainties are estimated with the aim of extending the results of these studies to the global atmospheric and oceanic circulation, both for the annual mean and annual cycle.

Fundamentals of the energy budget and key sources of uncertainty and error are presented and discussed by FT08 in the global mean context. The datasets are also described in detail in FT08. The purposes of the present manuscript are, therefore, 1) to explore the current range of estimates of the annual zonal mean energy budget and the mean annual cycle, 2) to quantify specific sources of uncertainty in the budget as a function of latitude and time of year by comparing results from different datasets and making estimates of the variability to assess sampling issues, and 3) to report the zonal mean characteristics of a comprehensive best estimate of the energy budget including quantification of the poleward transports by the ocean and atmosphere. The term best is used in the sense of "best practice"[1] in recognition of the fact that successive data and analyses are likely to improve upon the results presented here. The study is thus intended to serve as a baseline for evaluating coupled climate model simulations. As a detailed accounting of the considerations involved in constructing the best-estimate budget and its uncertainty is provided by FT08, only a brief discussion of the approach is provided here (section 2). Section 3 documents aspects of the meridional profiles of the annual zonal mean energy budget and the mean annual cycle, both for the globe and for land and ocean domains. The associated meridional transports of energy by the atmosphere and ocean are addressed in section 4 followed by a discussion of results and the conclusions (section 5).

## 2. Data and methods

More detailed discussion of the datasets, their characteristics, and analysis methods is given in FT08.

### a. Energy budgets

For the atmospheric energy $A_E$ (see FT08), the zonally averaged energy budget equation, when vertically integrated, can be written as

$$\overline{\frac{\partial A_E}{\partial t}} + \frac{1}{a\cos\phi}\frac{\partial[\overline{\mathbf{F}_A}]\cos\phi}{\partial\phi} = \overline{R_T} + \overline{F_S},$$

$$\text{where} \quad [\overline{\mathbf{F}_A}] = \int [\overline{\mathbf{v}(c_pT + gz + k + Lq)}]\, dp/g. \quad (1)$$

The overbar represents time averages and the [ ] depicts the zonal average across all longitudes. Here, $\mathbf{F}_A$ is the total vertically integrated atmospheric energy transport and only the meridional component remains after zonal averaging. The fields $k$, $T$, $\mathbf{v}$ $(=u, v)$, $q$, $p$, and $z$ denote the atmospheric kinetic energy, temperature, wind, specific humidity, pressure, and geopotential height, respectively. Standardized values $a$, $g$, $c_p$, and $L$, correspond to Earth's radius, the acceleration due to

[1] "Best practice" is a management idea that asserts a technique, method, or process is more effective at delivering a particular outcome than any other.

gravity, the specific heat of air at constant pressure, and the latent heat of vaporization, respectively. The terms in $[\mathbf{F}_A]$ consist of the meridional transport of the sensible heat, potential energy, kinetic energy, and latent energy, and the first two can be combined as the dry static energy, which combined with the last term, $Lq$, gives the moist static energy. The net upward surface flux is defined as $F_S$, and $R_T = \text{ASR} - \text{OLR}$.

As direct observations of $F_S$ over land are few, model simulations from the Community Land Model (CLM) forced by observed fields are used (Qian et al. 2006). Here, $F_S$ is inferred from the residual of the net downward TOA radiative flux ($R_T$) and the mass-corrected atmospheric total energy divergences and tendencies as per Trenberth (1997), such that

$$F_S = \partial A_E/\partial t + \boldsymbol{\nabla} \cdot \mathbf{F}_A - R_T. \tag{2}$$

We introduce the notation that a superscript corresponds to the domain: $g$ (global), $l$ (land), and $o$ (ocean). Thus, for the ocean, given $F_S^o$ and estimates of the vertically integrated ocean energy content $O_E$, the ocean divergence can be inferred based on

$$\boldsymbol{\nabla} \cdot \mathbf{F}_O = -F_S^o - \partial O_E/\partial t, \tag{3}$$

where

$$O_E = \int \rho T(z) C_w \, dz, \tag{4}$$

and here $z$ is the depth, $T$ is the ocean temperature, $\rho$ and $C_w$ are the density and specific heat of seawater, respectively, and the ocean energy is approximated by the ocean heat content.

### b. Adjusted satellite retrievals

Satellite retrievals from the Earth Radiation Budget Experiment (ERBE; February 1985–April 1989) and the Clouds and Earth's Radiant Energy System (CERES; March 2000–May 2004) are used to determine the TOA budget. These estimates are known to contain spurious imbalances (Wielicki et al. 2006). To match the available estimates of the global imbalance during the ERBE and CERES periods (Hansen et al. 2005; Willis et al. 2004; Huang 2006; Levitus et al. 2005), a number of adjustments are made to correct for unrealistically large $R_T$, as described in FT08. Future releases of updated CERES products may well improve upon the FT08 estimates. Associated uncertainty estimates, equal to two sample standard deviations of the interannual variability ($\pm 2\sigma_I$), are reported by FT08 in order to quantify the uncertainty associated with the limited temporal span of the ERBE and CERES time periods. Here, $\pm 2\sigma_I$ is similarly reported for zonal mean quantities. For all analysis of the in the current manuscript, these adjusted ERBE and CERES fields are thus used and in no instances are the raw retrievals used.

### c. Reanalysis datasets

In constructing estimates of the total atmospheric energy divergence and tendency, only fields strongly influenced by observations are used (e.g., Kalnay et al. 1996). These include surface pressure, atmospheric temperature, winds, geopotential height, and humidity from the National Centers for Environmental Prediction–National Center for Atmospheric Research (NCEP–NCAR) reanalysis (NRA; Kistler et al. 2001) and the 40-yr European Centre for Medium-Range Weather Forecasts (ECMWF) Re-Analysis (ERA-40; Uppala et al. 2005). All of the energy terms for the atmosphere, and their transports and divergences are computed as in Trenberth et al. (2001). Precipitation minus evaporation is computed from the atmospheric moisture budget rather than by differencing the model-derived fields of precipitation and evaporation (Trenberth and Guillemot 1998; Trenberth et al. 2001).

### d. Land model integrations

The seasonal variation of $F_S$ over land is taken from a stand-alone integration of the CLM (Bonan et al. 2002; Qian et al. 2006). The CLM represents the surface with five primary subgrid land cover types, 16 plant functional types, and 10 layers for soil temperature and water, with explicit treatment of liquid water and ice. Representation of the seasonal cycle by the CLM shows significant improvements over previous-generation models in regard to seasonality in surface air temperature, snow cover, and runoff (Dickinson et al. 2006). In the stand-alone integration used here, the CLM is forced with observed fields infilled with high-frequency information from the NRA where observations are unavailable (Qian et al. 2006). Values from the CLM are reported on a T42 grid, with 128 longitude and 64 latitude points, on a monthly basis from 1948 through 2004.

### e. Ocean surface fluxes and storage

The ocean datasets used to diagnose $T$ include the *World Ocean Atlas 2005* (*WOA*; Locarini et al. 2006), version 6.2 of the ocean analysis of the Japan Meteorological Agency (JMA; Ishii et al. 2006), and the recently corrected (6 February 2006) Global Ocean Data Assimilation System (GODAS; Behringer 2007); see FT08.

Estimates of $F_S^o$ are based on (2), whose accuracy is on the order of 20 W m$^{-2}$ over 1000-km scales (Tren-

berth et al. 2001) while satisfying closure among $F_S^o$, $\nabla \cdot \mathbf{F}_A$, $\delta A_E/\delta t$, and $R_T$. Because divergence is zero globally by definition, a cancellation of the error occurs over larger scales, and thus errors in $\nabla \cdot \mathbf{F}_A$ are largely random. Uncertainty in $F_S^o$ is thus governed by the uncertainties in $R_T$, $\nabla \cdot \mathbf{F}_A$, and $\delta A_E/\delta t$, which are frequently much less than those associated with other estimates of surface radiative and turbulent fluxes (see Trenberth et al. 2001 and FT08). FT08 identify an excessive annual cycle of $O_E$ in JMA and *WOA* relative to that which can be explained by either a range of $F_S^o$ estimates or GODAS fields. It thus remains an outstanding science question investigated here as to the spatial patterns that are associated with these biases in $O_E$ and whether the patterns are suggestive of the underlying causes of the biases.

### *f. Regridding and standard deviations*

To provide a consistent delineation of the land–sea boundaries among the various datasets described above, all fields are transformed to a grid containing 192 evenly spaced longitudinal grid points and 96 Gaussian-spaced latitudinal grid points using bilinear interpolation (i.e., to a T63 grid). Spatial integrals are calculated using Gaussian weights over the T63 grid and a common land–sea mask is applied. Total energy is expressed in units of petawatts (PW; 1 petawatt = $10^{15}$ W) and monthly mean values are used for all calculations. In quantifying seasonal variability, the estimated population standard deviation of monthly values is used.

## 3. The zonal mean energy budget

To ensure conservation of energy and to provide a representative portrayal of the magnitudes of the terms in the energy budget, we deal with actual areally integrated amounts, generally expressed in terms of petawatts rather than watts per square meter. The conversion globally is 1 W m$^{-2}$ = 0.510 PW, over the global ocean it is 1 W m$^{-2}$ = 0.372 PW, and over the global land it is 1 W m$^{-2}$ = 0.138 PW. For zonal means, the integrals better depict the meridional structure. Rather than use per meter as the remaining dimension, we have chosen to use 1° latitude, as 111.3 km. Thus, the units are petawatts per degree. In most figures, the annual mean value is removed to reveal departures and the annual mean is presented separately.

For albedo, ASR, and OLR, both the annual cycle (Figs. 1a–c) and the annual zonal mean (Fig. 1d) are plotted with hatched and stippled regions representing areas of significant discrepancies between ERBE and CERES best-estimate fields exceeding both $\pm 2\sigma_I$ and 5 W m$^{-2}$ (or 0.02 in the case of albedo). Monthly mean albedo (Fig. 1a) is characterized by the largest variability in the polar regions, but the variability is also large in the midlatitude Northern Hemisphere, and with winter maxima in each hemisphere. In the tropics, the seasonality of the albedo for each hemisphere is out of phase with the higher latitudes and is associated with changes in cloud and thus OLR (Fig. 1c). CERES albedo estimates are less than those of ERBE across the tropics and subtropics, and are greater than those of ERBE only in the Southern Hemisphere polar regions in May–August, when solar irradiance is very small. The annual cycle of ASR (Fig. 1b) is dictated to first order by the seasonal migration of solar irradiance and, secondarily, by albedo and its variability. Peak seasonal variability in ASR is evident at approximately 40° in each hemisphere.

The amplitude of the mean seasonal cycle of OLR (Fig. 1c) is approximately 20% of that of ASR (note the reduced contour scale). In the midlatitudes, the seasonal cycle of OLR lags ASR in phase by 1–2 months, reflecting the phase lag between the influences of radiative heating (i.e., ASR) and surface temperature (that influences strongly OLR). In the tropics, OLR is instead dominated by high cloud variations associated with the seasonal migration of the intertropical convergence zone (ITCZ) and the monsoon trough, and thus the annual cycle of OLR is out of phase with the midlatitude variability. The monsoon's influences create increased OLR during the dry season when clouds are few and decreased OLR when convection and deep cloud occur in the wet season (Fig. 1a). CERES OLR estimates significantly exceed those of ERBE north of 25°N and in the southern tropics during austral winter. For the zonal annual mean (Fig. 1d), the OLR differences in the southern tropics are the dominant contributors to the ERBE–CERES differences.

The mean albedo (Fig. 1d) is lowest in the tropics at 20%–30%, increasing to 30% in the subtropics, 40% in the midlatitudes, and 50%–70% poleward of 60°. ASR is greater than OLR from about 35°S to 35°N and the imbalance is compensated for by energy transports from the tropics by the ocean and atmosphere. Meanwhile, OLR exceeds ASR in the mid- and high latitudes, contributing to a TOA net radiative deficit there that is balanced by $F_S$ and $\nabla \cdot \mathbf{F}_A$. These meridional transports are addressed in section 4.

Figure 2 summarizes the zonal mean annual cycles of $R_T$, $\delta A_E/\delta t$, $\nabla \cdot \mathbf{F}_A$, and $F_S$, plotted on a common scale with the differences between the estimates highlighted where they exceed $\pm 2\sigma_I$. At the TOA, consistent with the lower albedo, CERES data depict a larger net in-

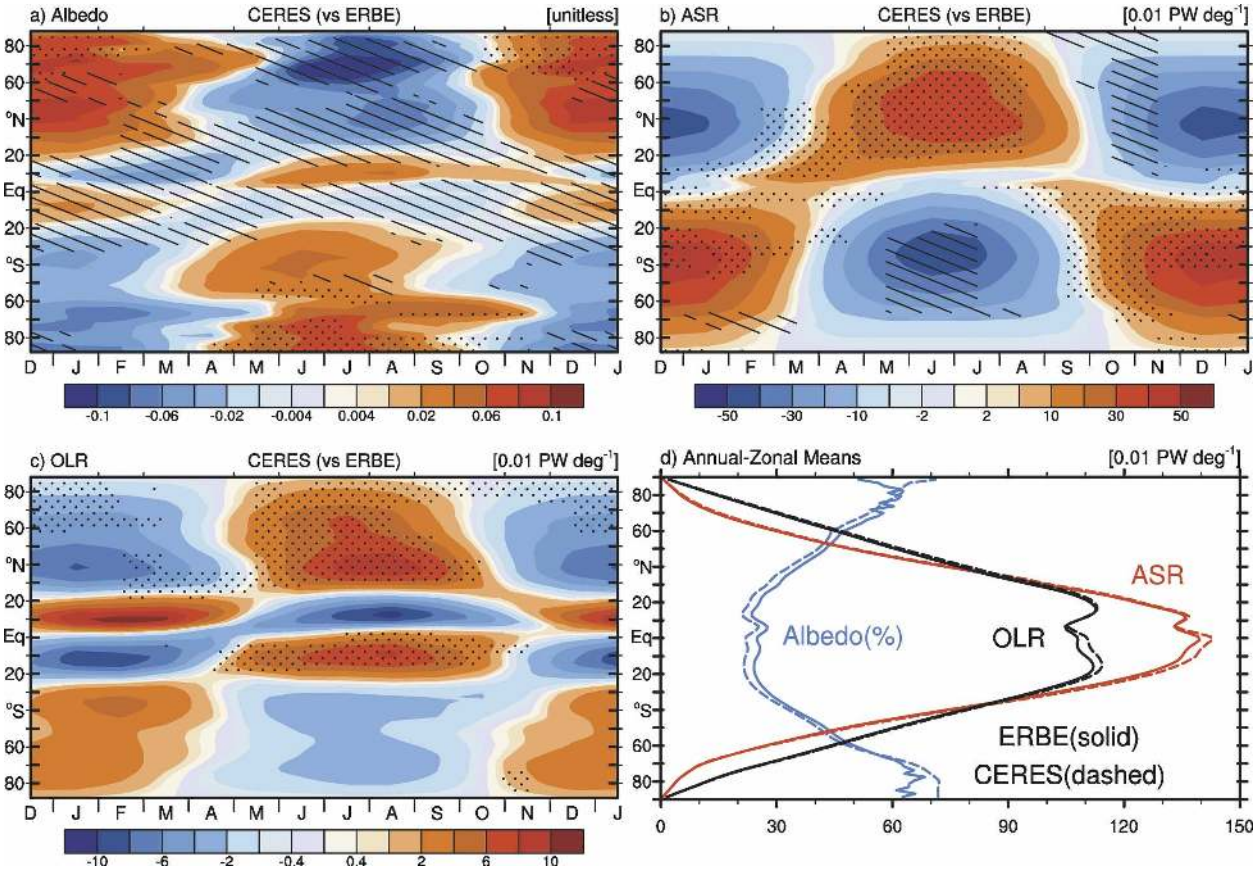


FIG. 1. Zonal mean departures from the annual mean of (a) albedo (fraction), (b) ASR, and (c) OLR are shown based on CERES retrievals with positive (negative) differences from ERBE fields stippled (hatched) where they exceed $\pm 2\sigma_I$ and $\pm 5$ W m$^{-2}$ (or $\pm 0.02$ in the case of albedo). (d) The zonal annual mean terms as a function of latitude. The CERES values are based on averages from March 2000 to May 2004, the CERES period, while ERBE values are based on averages from February 1985 through April 1989, the ERBE period. For ASR and OLR the units are 0.01 PW $(^\circ)^{-1}$.

coming flux than do the ERBE data in the summer hemisphere and subtropical winter domains (Figs. 1b and 1c). As for ASR, peaks in seasonal variability in $R_T$ occur near 35° latitude in each hemisphere. As estimates of $\delta A_E/\delta t$ are small and agree generally among the datasets, the primary source of discrepancies in the zonal mean atmospheric budgets is $\nabla \cdot \mathbf{F}_A$, which is stronger in ERA-40 than NRA in the deep tropics and weaker in the northern subtropics. However, these differences are not often larger than $\pm 2\sigma_I$ and thus are within the sampling error. The zonal mean seasonal cycle of $F_S$ is characterized by strong net upward (downward) flux during local winter (summer) that is of comparable magnitude to $R_T$ with differences between the estimates that are spatially similar to those in $\nabla \cdot \mathbf{F}_A$.

The zonal annual mean energy budget for the ERBE, CERES, ERA-40, and NRA fields (Fig. 3) reveals that $R_T$ is greatest in the tropics [$\sim$0.3 PW $(^\circ)^{-1}$ or $\sim$67 W m$^{-2}$] and near zero at 35°, poleward of which $R_T$ is negative. The disparity in $R_T$ between CERES and ERBE is most pronounced in the tropics and exceeds 0.03 PW $(^\circ)^{-1}$ (up to 10 W m$^{-2}$), or over 10%, in the zonal mean at some latitudes. Except for the deep tropics, the zonal mean structure of $\nabla \cdot \mathbf{F}_A$ resembles that of $R_T$ and is characterized by positive values in the tropics and subtropics [$\sim$0.2 PW $(^\circ)^{-1}$ or $\sim$45 W m$^{-2}$] and negative values poleward of 40°. While the differences between the $R_T$ estimates in the tropics are considerable, discrepancies in $\nabla \cdot \mathbf{F}_A$ between the NRA and ERA-40 estimates, which peak in the subtropics and deep tropics, are of similar magnitude for the ERBE period. Limitations in the ability of the reanalyses to accurately resolve $\nabla \cdot \mathbf{F}_A$, and by extension $F_S$, as a function of latitude are thus highlighted. Relative to $\nabla \cdot \mathbf{F}_A$, the zonal annual mean of $\delta A_E/\delta t$ is small [$<$0.01 PW $(^\circ)^{-1}$ or $<$3 W m$^{-2}$] at all latitudes and differences between the estimates thus contribute only marginally to the uncertainty in $F_S$.

For the annual means (Fig. 3), at the surface in the

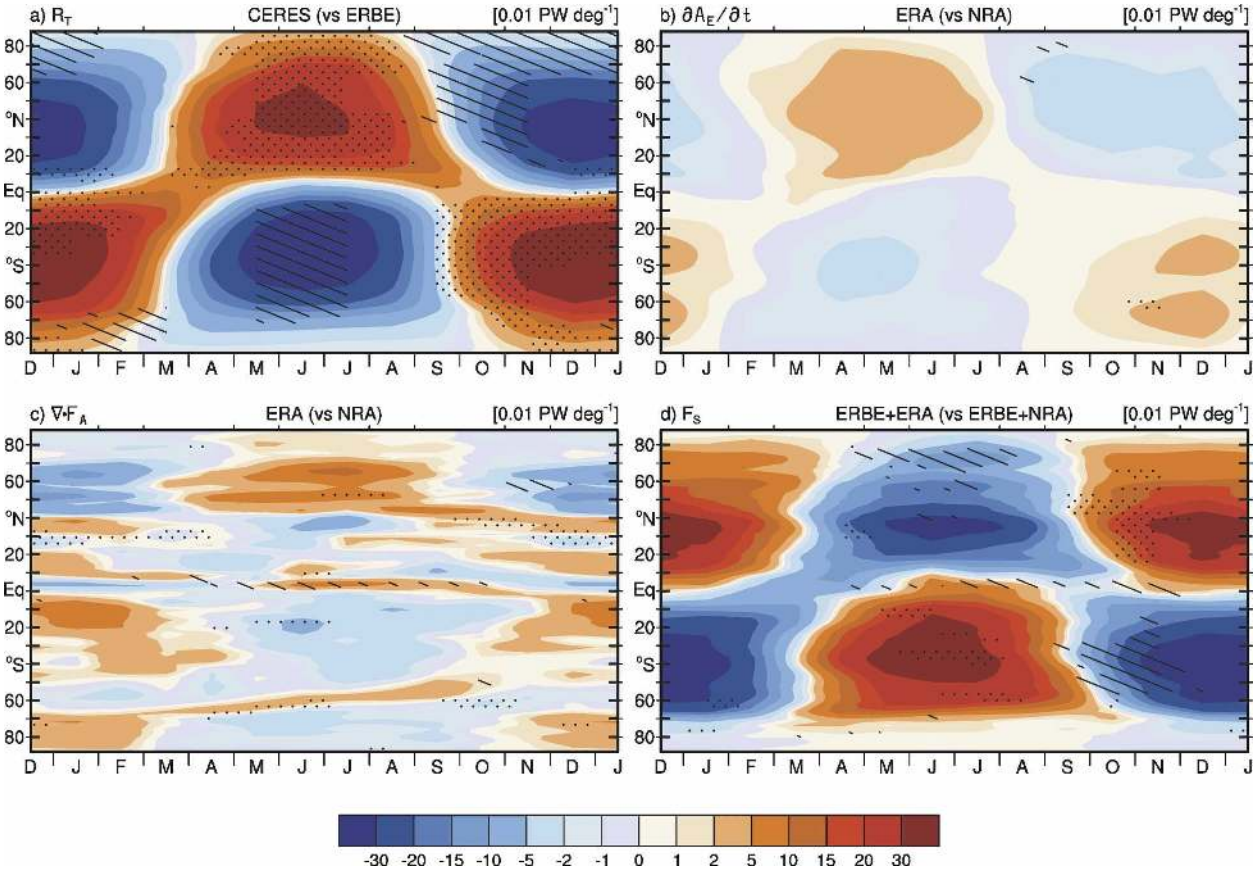


FIG. 2. Zonal mean monthly deviations from the annual mean [$\times$0.01 PW $(°)^{-1}$] are shown for (a) $R_T$, (b) $\delta A_E/\delta t$, (c) $\nabla \cdot \mathbf{F}_A$, and (d) $F_S$. Stippling (hatching) is used to indicate regions in which the flux plotted exceeds (falls below) companion estimates, indicated in parentheses, by $\pm 2\sigma_I$ and $\pm 5$ W m$^{-2}$. For all fields, the time period considered is the ERBE period except for CERES $R_T$, for which the CERES period is considered.

tropics, $F_S$ peaks at about $-0.25$ PW $(°)^{-1}$ ($-55$ W m$^{-2}$) on the equator. Within 10° of the equator however, $\nabla \cdot \mathbf{F}_A$ more than doubles its equatorial value and the energy flux into the ocean decreases rapidly with latitude, reaching zero equatorward of 20° for all estimates. In the subtropics (20°–40°), a mean net upward flux of energy at the surface is also evident, peaking at 0.12 PW $(°)^{-1}$ (30 W m$^{-2}$) at 35°N and at 0.06 PW $(°)^{-1}$ (15 W m$^{-2}$) near 30°S for the NRA–ERBE estimates. As shown in Trenberth and Stepaniak (2003a,b), $F_S$ at these latitudes is composed largely of the latent energy evaporative flux. North of 40°N the annual zonal mean surface flux is small relative to $\nabla \cdot \mathbf{F}_A$. However, in the Southern Hemisphere, a second maximum in $F_S$ of 0.06 PW $(°)^{-1}$ ($\sim$25 W m$^{-2}$) is apparent near 65°S and is likely to be associated with cold air drainage of low-enthalpy katabatic surface outflow from Antarctica over the southern oceans (Trenberth and Stepaniak 2003b).

The zonal mean annual cycles of the anomalies for land (Fig. 4) and ocean (Fig. 5) show that the integrated fluxes are generally greater over ocean than over land as the areal extent of ocean exceeds that of land at most latitudes. Moreover, the latitudinal structures of the land and ocean budgets are influenced by their geographic distributions (i.e., Northern Hemisphere for land and Southern Hemisphere for ocean). Because $F_S$ over land is very small, the principle energy balance in Fig. 4 is achieved between $R_T$ and $\nabla \cdot \mathbf{F}_A$ with convergence (divergence) of energy in winter (summer). In contrast, over ocean (Fig. 5) the balance is predominantly between $R_T$ and $F_S$, with $\nabla \cdot \mathbf{F}_A$ and $\delta A_E/\delta t$ playing important but secondary roles.

The structure and phase of the zonal mean annual cycles of $R_T$ and $\delta A_E/\delta t$ over ocean (Figs. 5a and 5b) are similar to those over land, with the phase of $F_S$ over ocean (Fig. 5d) matching closely that of $R_T$, while $\nabla \cdot \mathbf{F}_A$ over ocean is largely out of phase with (i.e., balancing) that over land at all latitudes. In Northern Hemisphere subtropics and midlatitudes, where the largest values of $\nabla \cdot \mathbf{F}_A$ over ocean occur, the $\nabla \cdot \mathbf{F}_A$ and

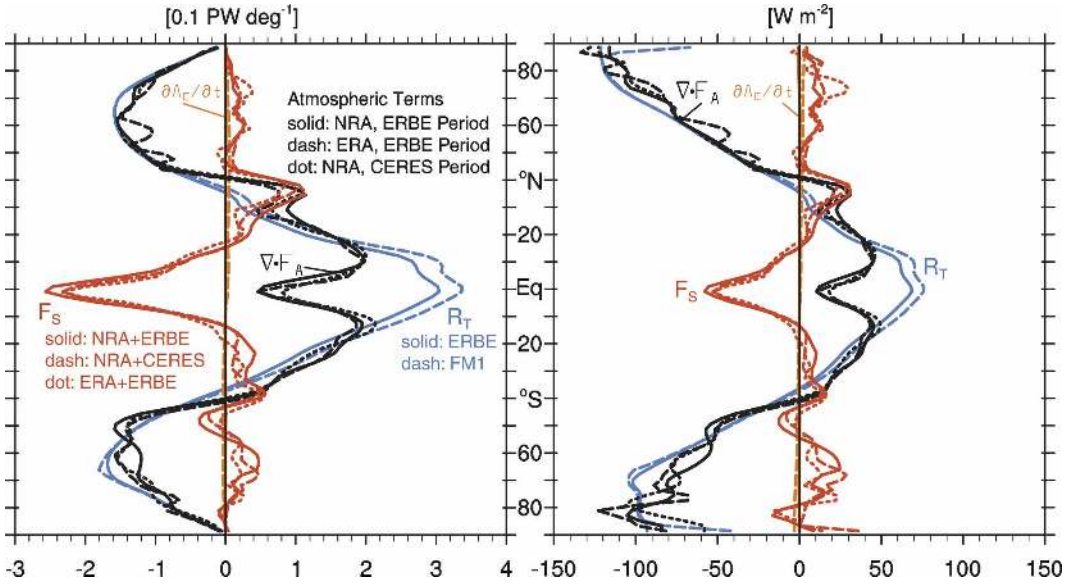


FIG. 3. Zonal annual mean TOA $R_T$, atmospheric $\nabla \cdot \mathrm{F_A}$, and surface terms $F_S$ [$\times 0.01$ PW $(^\circ)^{-1}$] for the ERBE and CERES periods are shown where available based on combinations of NRA or ERA-40 with ERBE or CERES data.

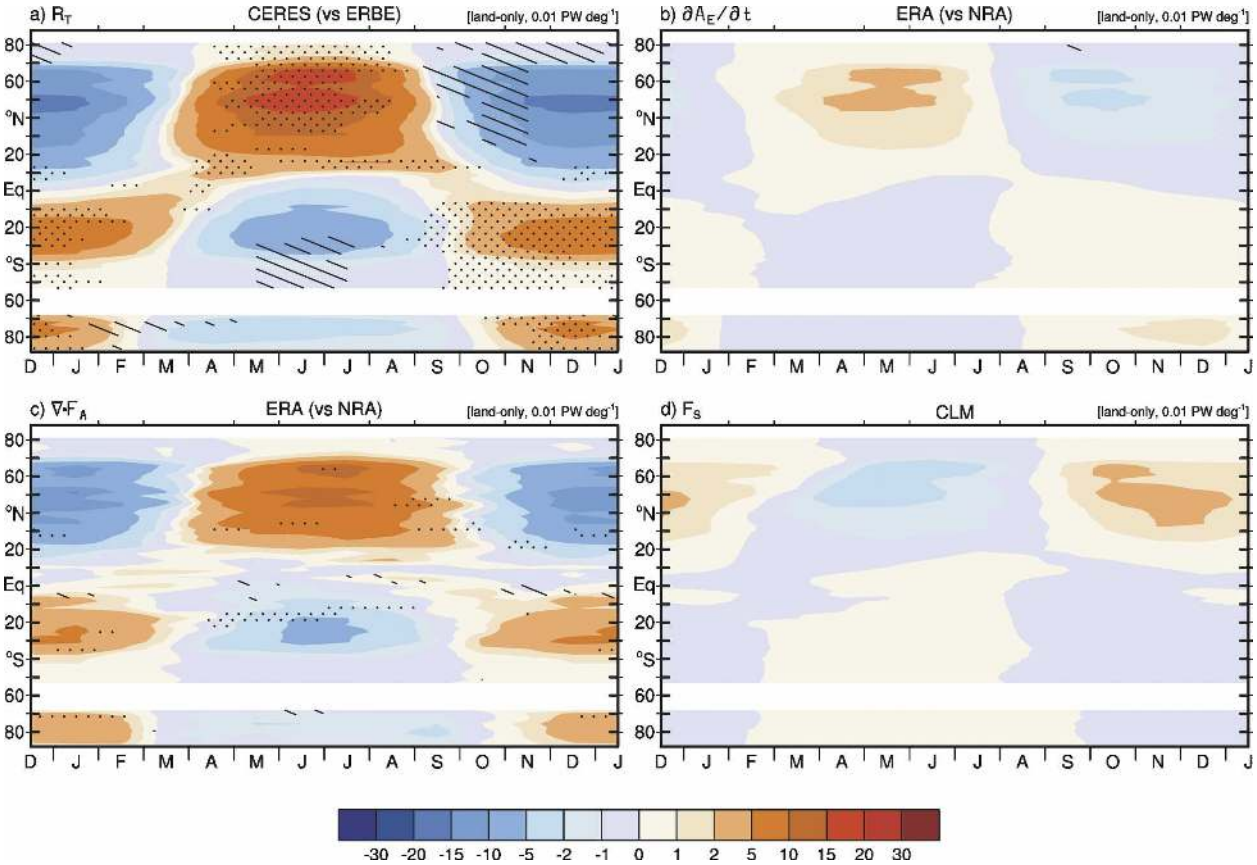


FIG. 4. For the land domain, zonal mean monthly deviations from the annual mean [$\times 0.01$ PW $(^\circ)^{-1}$] are shown for (a) $R_T$, (b) $\delta A_E/\delta t$, (c) $\boldsymbol{\nabla} \cdot \mathbf{F}_A$, and (d) $F_S$. Stippling (hatching) is used to indicate regions in which the flux plotted exceeds (falls below) companion estimates, indicated in parentheses, by $\pm 2\sigma_I$ and $\pm 5$ W m$^{-2}$. For all fields, the time period considered is the ERBE period except for CERES $R_T$, for which the CERES period is considered.

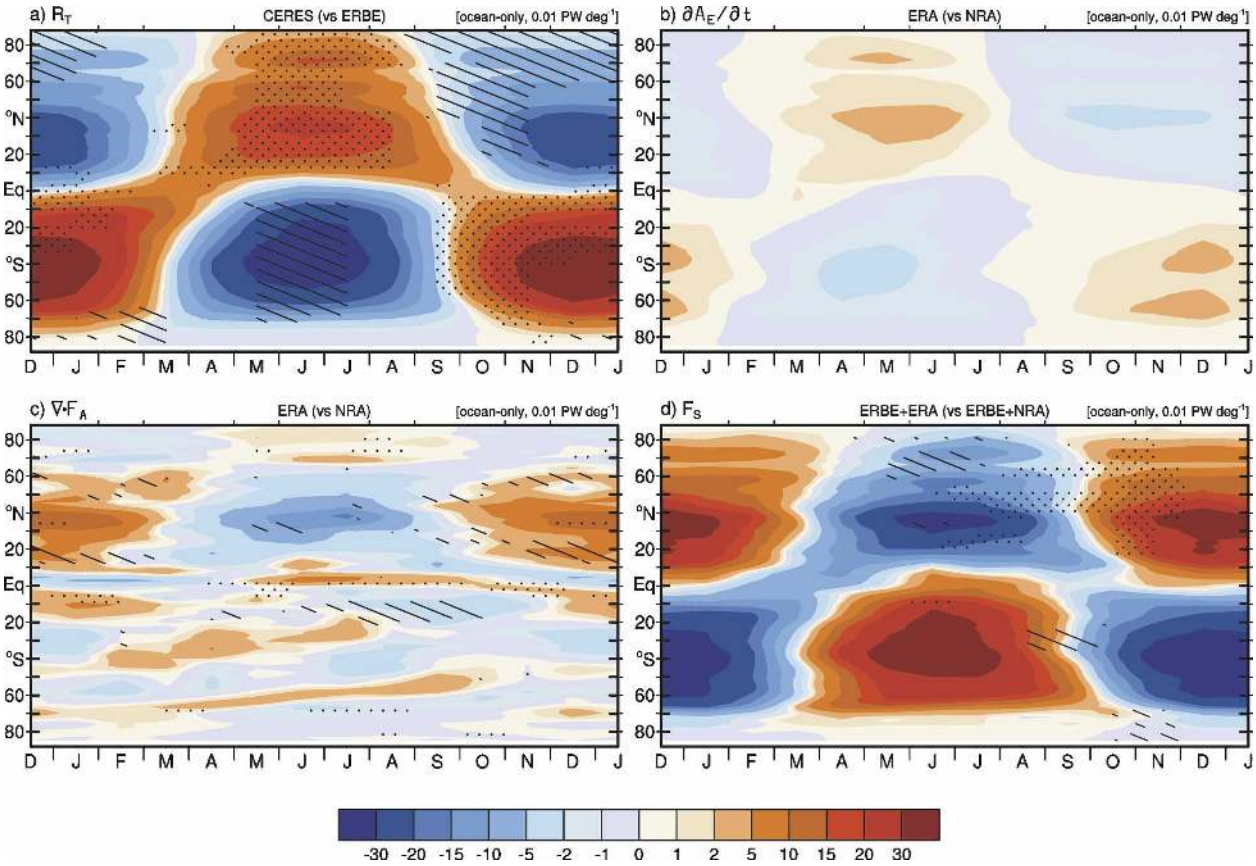


FIG. 5. As in Fig. 4, but for the ocean domain.

$F_S$ variabilities are of the same sign, as in winter (summer) there exists a divergence (convergence) in the midlatitudes relative to the annual mean, and the seasonal variability of $F_S$ is therefore larger than would be expected based on $R_T$ alone.

A significant finding of FT08 was the excessive global ocean heat content $O_E$ annual cycle reported by in situ data relative to $F_s$ and, in particular, by JMA and *WOA*. To identify the regions contributing most significantly to the bias, Fig. 6 shows the zonal annual mean and monthly mean annual cycle of $O_E$ for 1990–99, the decade for which the observations incorporated into *WOA* and JMA are most numerous. As the seasonal cycle of the zonal mean $\nabla \cdot \mathbf{F}_O$ is not well known, it is not possible to infer the zonal mean annual cycle of $O_E$ from $F_S$ in (3), and therefore direct computations of the energy budget cannot be included in Fig. 6. Nonetheless, some important characteristics are noted. Figure 6a shows both the zonal annual mean and the standard deviation of the mean annual cycle ($\sigma$). The *WOA* and JMA annual mean latitudinal profiles agree quite well, which is not surprising as they are based upon a similar set of observations, and both are cooler than the GODAS fields at all latitudes by approximately 20%. This appears to be a fairly systematic offset or bias related to the different analysis procedures, as the magnitude of the annual cycle of the zonal means estimated from $\sigma$ is very similar among the datasets, with weak variability in the tropics and strong midlatitude variability peaking at 40° in both hemispheres. The greatest differences between the estimates of $\sigma$ exist near 50°S, where the ocean extent is considerable, and where the GODAS variability is significantly less than that of JMA and *WOA*. The seasonal character of these differences is shown in greater detail in Figs. 6b and 6c where stippling (hatching) is used to show times and places for which the *WOA* and JMA estimates significantly exceed (fall below) those of GODAS.

While some differences between the datasets exist in the Northern Hemisphere, the overwhelming majority of the discrepancies occur in the Southern Hemisphere and especially south of 40°S, with both *WOA* and JMA biases from GODAS contributing to excessive Southern Hemisphere seasonal variability for the ocean as a whole. The regions highlighted in Fig. 6 are also notorious for being data sparse (e.g., Locarnini et al. 2006).

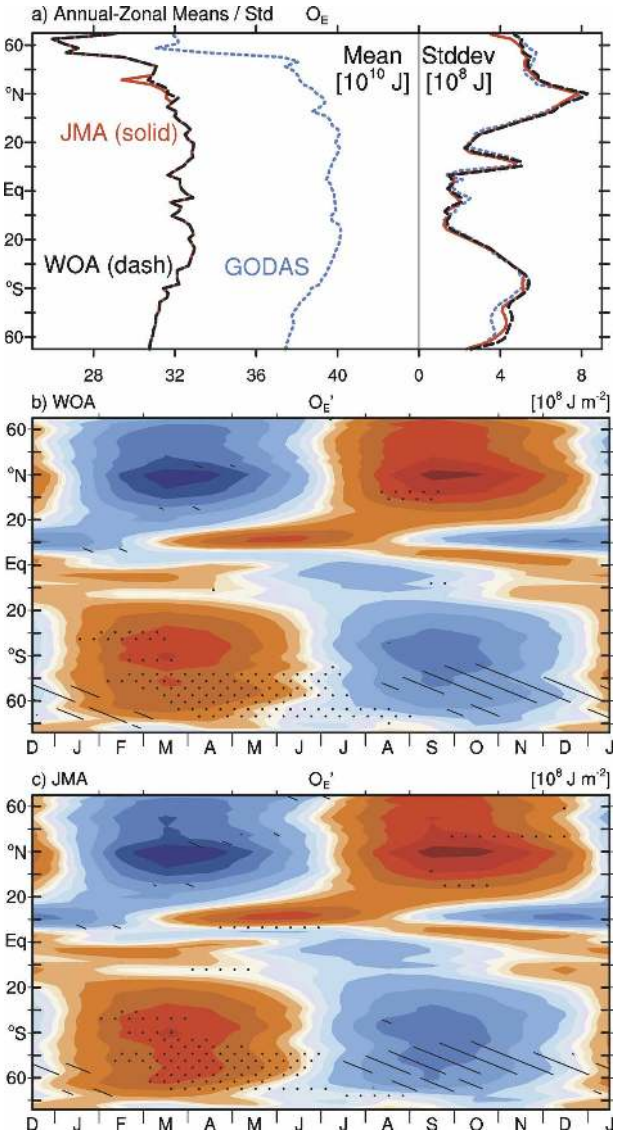


FIG. 6. (a) Annual zonal means ($\times 10^{10}$ J m$^{-2}$) (left) and standard deviations (right) of $O_E$ for the *WOA*, JMA, and GODAS datasets. Zonal mean $O_E$ departures ($\times 10^8$ J m$^{-2}$) from the annual mean are shown for (b) *WOA* and (c) JMA. The GODAS and JMA fields from 1990 to 1999 are used while the *WOA* monthly climatology is used. Differences in (b) *WOA* vs GODAS, and (c) JMA vs GODAS, show hatched (stippled) regions indicating the regions in which *WOA* and JMA are significantly greater than (less than) the GODAS monthly climatology [here an uncertainty range of $\pm 2\sigma_I$ (10 yr)$^{-1/2}$ from GODAS is used]. The units are $10^{10}$ or $10^8$ J m$^{-2}$ for the mean and departures, respectively.

The net result of the differences is to increase the global mean $O_E$ maximum in March–May and decrease the $O_E$ minimum from August through November, biases that agree closely with the seasonality of biases in the global ocean budget identified in FT08. Together, these differences result in notably stronger global ocean annual cycles in JMA and *WOA* compared with GODAS (Fig. 7a in FT08), which is not consistent with the observed surface and TOA energy budgets.

## 4. Meridional energy transports

The zonal mean meridional transports and their uncertainties are calculated by integrating the atmospheric divergences with latitude using ERBE estimates at the TOA, $\delta A_E/\delta t$ and $\nabla \cdot \mathbf{F}_A$ estimates from NRA, and the oceanic divergences from GODAS using (3) (Fig. 7). For the annual cycle, the uncertainty is based on the standard deviation ($\sigma$) among several monthly mean transport estimates. For the atmosphere, these estimates are ERA-40 and NRA for the ERBE period and NRA for the CERES period. For the ocean, each of the three separate estimates of the atmospheric budgets is combined with the ERBE and CERES estimates of $R_T$, and estimates of $\delta O_E/\delta t$ from GODAS for the ERBE and CERES periods. Uncertainty estimates thus include a contribution from the different sources of data in addition to the interannual variability characterized by ERBE and CERES period differences. As the JMA and *WOA* fields have been shown to be deficient in the Southern Hemisphere (Fig. 6), only the GODAS fields are used to estimate $\delta O_E/\delta t$ in Fig. 7.

The annual cycle of the total poleward transport (Fig. 7a) is characterized by peak transport in the winter hemisphere that exceeds 8 PW in December for the Northern Hemisphere and 7 PW from June through September in the Southern Hemisphere. The summer transports are relatively weak and peak near 3 PW for the Northern Hemisphere and 2 PW for the Southern Hemisphere. Midlatitude transports are dominated by the atmosphere (Fig. 7b), and exceed 6 PW at 40°N and 5 PW at 40°S in winter. In the summer, the Southern Hemisphere poleward transports are somewhat greater (>3 PW) than in the Northern Hemisphere. Global ocean transports (Fig. 7c) are small outside of the tropics and vary in phase generally with higher-latitude winter atmospheric transports, although with early and late season northward peaks in December, March, and April, and a southward peak in September that extends into the northern tropics. Tropical poleward transport exceeds 2 PW from November through March north of the equator, peaking at 5 PW in December. South of the equator, this transport exceeds 2 PW from March through October and peaks at 4 PW in September. While atmospheric transports are as large as or larger than those of the ocean for most regions and months, interhemispheric transports consist of important contributions from both the atmosphere and ocean, and

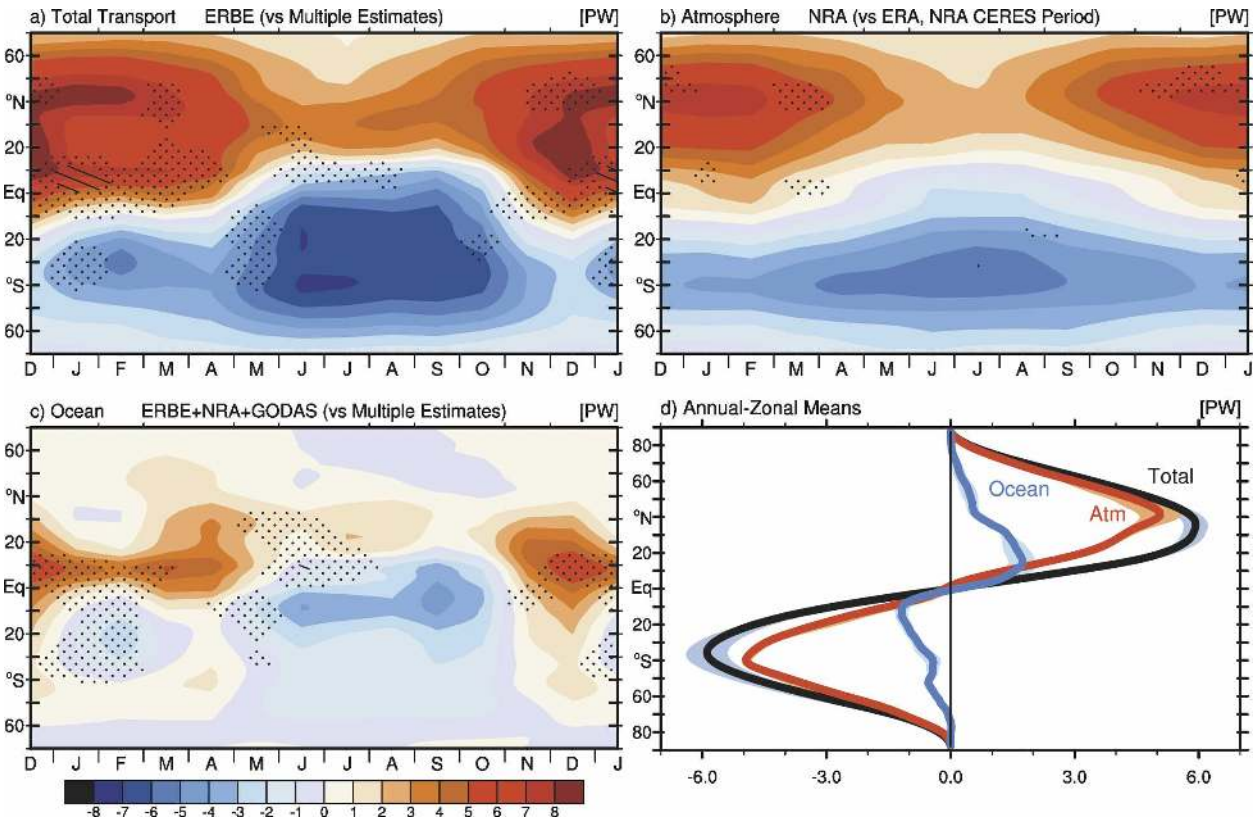


FIG. 7. The ERBE period zonal mean annual cycle of the meridional energy transport in PW by (a) the atmosphere and ocean as inferred from ERBE $R_T$, NRA $\delta A_E/\delta t$, and GODAS $\delta O_E/\delta t$; (b) the atmosphere based on NRA; and (c) by the ocean as implied by ERBE + NRA $F_S$ and GODAS $\delta O_E/\delta t$. Stippling and hatching in (a)–(c) represent regions and times of year in which the standard deviation of the monthly mean values among estimates, some of which include the CERES period (see text), exceeds 0.5 and 1.0 PW, respectively. (d) The median annual mean transport by latitude for the total (gray), atmosphere (red), and ocean (blue) accompanied with the associated $\pm 2\sigma$ range (shaded).

cross-equatorial transports are characterized by flows from the summer to winter hemispheres that exceed 4 PW in most months. In the regions of maximum transport, uncertainty among the estimates is generally less than 0.5 PW. The uncertainty in the monthly mean transports is greatest in the tropics and exceeds 1 PW in the equatorial ocean in June and July where the uncertainty in the atmospheric transports is also a maximum and exceeds 0.5 PW.

The annual zonal mean total transport (Fig. 7d) can be inferred from the ERBE and CERES fields directly, as the tendency terms are relatively small. The peak total transport of 5.9 PW exists at 35° in both hemispheres with a $\pm 2\sigma$ range of 0.5 PW in the Southern Hemisphere and 0.3 PW in the Northern Hemisphere. Transport in the atmosphere peaks at 5.1 PW at 41°N and 4.9 PW at 39°S with a $\pm 2\sigma$ range of 0.5 and 0.2 PW in the Northern and Southern Hemispheres, respectively. Mean global ocean transport maxima occur at 15°N (1.7 PW) and 11°S (1.2 PW) where the associated $\pm 2\sigma$ ranges are 0.3 and 0.5 PW, respectively.

## 5. Discussion and conclusions

The zonal mean energy budget and its annual cycle for the globe and for land and ocean domains have been examined and the associated meridional transports of energy by the atmosphere and ocean have been computed. The primary means of indicating sources of errors is the reproducibility of the results across various datasets. Physical constraints have been used to either remove the largest systematic errors or indicate where results are not viable, and one component of the uncertainty, namely that associated with sampling, is estimated. Removing the systematic error may underestimate the total uncertainty in any value but it nonetheless provides a better assessment of the state of knowledge with regard to energy flows. Note that the systematic error was removed by adjusting the albedo and thus ASR, and is therefore not constant in latitude. In contrast, Wunsch (2005) unrealistically treats the estimated error in the net radiation as random although meridional transports are constrained by the global bal-

ance, and he finds one standard deviation error bars in both the TOA ERBE total transports and the atmospheric meridional transports exceeding 1 PW in both hemispheres.

In the extratropics, ASR achieves a maximum in the summer with peak values near the solstices. The OLR maxima also occur in the summer but lag by 1–2 months, which is more consistent with the temperature maxima over land. In the tropics, however, OLR relates more to high cloud variations and thus the maxima occur in the late winter, which is the dry monsoon season with suppressed clouds and elevated surface temperatures. In contrast, the minimum in summer coincides with deep convection in the monsoon trough at the peak of the rainy season. Most of the difference between the TOA radiation and the atmospheric energy storage tendency results in a large heat flux into the ocean in summer, along with a substantial transport from ocean to land in winter (Figs. 3, 4c, and 5c). A smaller transport occurs from land to ocean in summer in the Northern Hemisphere extratropics and throughout the tropics, as seen in Figs. 4c and 5c, and Fig. 5 of FT08. In the extratropics of the Southern Hemisphere, land–ocean differences play only a small role and the main energy transport is poleward.

At the TOA the importance of the errors in the retrieval process in achieving a more precise depiction of the budget are identified, particularly in regard to albedo and ASR in the tropics. These shortcomings are highlighted as fundamental to the limitations on our current budget estimates. Differences between the ERA-40 and NRA estimates of $\nabla \cdot \mathbf{F}_A$ obscure further key aspects of the atmospheric, surface, and, by extension, oceanic budgets. However, the largest disparities in the energy budget arise from the estimation of $O_E$ using the *WOA* and JMA fields. Beyond the likely ranges of error in $F_S$, it is found that the annual cycles of global ocean $O_E$ in these fields greatly exceed those that can be explained by surface forcing, even when likely error bounds are considered. Comparison with GODAS fields shows the main discrepancies to exist in the Southern Hemisphere mid- to high latitudes (Fig. 6). As these discrepancies coincide with major gaps in the observational record exploited by JMA and *WOA*, it is thus suggested that the in situ record in these infilled regions is very likely spurious; this record has also been cited as being a cause for concern in independent comparisons with model fields (AchutaRao et al. 2006). Moreover, the likely uncertainties in ocean heat storage, especially in the Southern Hemisphere, found here can alter the apparent trends if the ocean observing system changes, as it has in recent years with Argo floats, and may be one source of the discrepancy between the ocean heat content changes (Gouretski and Koltermann 2007) and sea level changes (Lombard et al. 2007). Moreover, the GODAS fields, which rely on model-simulated fields rather than infilling, agree more closely with tendencies derived from independent estimates of $F_S$.

Among the few analyses to report monthly meridional ocean transports, OV76 estimate ocean transports only in the Northern Hemisphere as a residual using only radiosonde data in the atmosphere, rather than global analyses, and the data are deficient over the oceans, leading to atmospheric transports that were much too low. The phase of the annual cycle reported by OV76 resolves the existence of the summer minimum and winter maximum in transport shown in Fig. 7b; however, the monthly mean magnitudes of the transport are understated by approximately a factor of 2 for all months and latitudes. The disagreements of our results with OV76 lie well outside of the range of uncertainty (hatching/stippling in Fig. 7c) and arise from our inclusion of multiple data sources in our estimates, the much more extensive period, and the more comprehensive sampling of the mean state and range of the uncertainty. Differences with Zhang and Rossow (1997) arise from their dependence on explicit calculations of surface fluxes that rely on assumptions regarding aerosol concentrations, cloud droplet size, and other key parameters, which are likely to contain considerable systematic and sampling errors.

In this study we have treated the two atmospheric reanalyses as equals. However, from the standpoint of the energy budget, the ERA-40 is further removed from satisfying our basic constraints and it is known to have serious errors in the tropics in the hydrological cycle (Uppala et al. 2005; Trenberth et al. 2005); see also FT08. More generally, significant caveats with the atmospheric budget remain primarily in the representation of the hydrologic cycle, particularly with regard to precipitation. These uncertainties are greatest in the atmospheric transports in the deep tropics where precipitation rates are large, and the divergent atmospheric circulation plays a major role (Trenberth et al. 2007).

The annual cycle of the atmospheric transports reflects the seasonality in the equator-to-pole temperature gradients, which peak in the winter hemisphere and therefore drive stronger meridional circulations and transports of energy through baroclinic eddies, stationary waves (in the Northern Hemisphere) from the hemispheric asymmetry of the land distribution, and the Hadley circulation (Trenberth and Stepaniak 2003a,b). These processes contribute to greater seasonality in the atmospheric divergence in the Northern

Hemisphere (Figs. 4, 5, and 7). Therefore, the maximum poleward transports peak in the winter hemisphere, both for the atmosphere at all latitudes and for the tropical oceans, and the range in monthly mean transports across the mean annual cycle is found to be of similar magnitude to the annual mean transport itself. For most regions, the uncertainty in the monthly mean atmospheric and oceanic transports is less than 0.5 PW and the tropical regions are identified as regions where differences exceed this limit. In relating the zonal mean energy divergences in the atmosphere and ocean to the net transports, the estimates here are generally consistent with prior assessments of the mean atmospheric transport that rely on the residual method for deriving $F_S$ (Trenberth and Caron 2001).

The dominance of atmospheric transports over oceanic transports outside of the tropics is expected based on theoretical constraints that relate the relative roles of the transports to the ratio of the heat capacity of the water and air scaled by the ratio of the moist- to the dry-adiabatic lapse rates near the surface, a scaling that increases with latitude (Held 2001; Czaja and Marshall 2006). Indeed, this relationship has been validated by several previous observational studies and is verified here to be valid beyond the bounds of likely uncertainties. Moreover, the key role of the oceans in the meridional transport of energy in the deep tropics is also confirmed.

A potentially important aspect of the annual cycle of the ocean transport that has not been addressed here pertains to the seasonal variability of the sea ice distribution, for which reliable estimates of total ice volume and mass, and thus the total latent heat of fusion, are unavailable. With the accumulation of sea ice in autumn and winter, when the ocean temperature is falling, the surface flux is large out of the ocean and reverses in spring and summer when ocean temperatures increase and melting occurs. These aspects are explored in considerable detail by Serreze et al. (2007), who show that the vertically integrated net transport of the atmospheric energy into the polar cap north of 70°N from ERA-40 is 1.4 PW (100 W $m^{-2}$) in the annual mean for 1979–2001. For the ocean domain, the July net surface flux from ERA-40 of 1.2 PW into the ocean (−100 W $m^{-2}$) associated with sea ice melt and oceanic sensible heat gain is less than the atmospheric convergence of 1.3 PW (91 W $m^{-2}$). During winter, oceanic sensible heat loss and sea ice growth yield a flux from the Arctic Ocean to the atmosphere of 0.6–0.7 PW (50–60 W $m^{-2}$) complemented with an atmospheric convergence of 1.1–1.3 PW (80–90 W $m^{-2}$) to provide a radiative loss to space of 2.5 PW (175–180 W $m^{-2}$). Serreze et al. (2007) estimate the uptake and release of energy in forming and melting ice to range from −0.6 to +0.8 PW (−48 to +69 W $m^{-2}$) over the polar cap.

It is therefore likely that the annual cycle of the transport into regions of seasonal sea ice is overestimated in Fig. 7. FT08 estimate that the magnitude of this energy flux in the Arctic can be on the order of 0.5 PW although the uncertainty associated with this value is large. The omission of the energy transport associated with sea ice for the annual mean is significantly smaller, however, as the accumulated energy associated with the melting of sea ice is a secondary component of the long-term budget (Levitus et al. 2005).

The holistic evaluation of the TOA, atmospheric, surface, and ocean energy budgets presented here has assisted in evaluating the energy budget, its key flows and balances, and its outstanding uncertainties to a degree that would not be possible with any single dataset. Nonetheless, it is through the ongoing efforts of specialized groups, such as the NASA CERES team and the groups constructing synthesized datasets, such as the atmospheric reanalyses and ocean atlases, that an improved understanding of the energy budget will be attained. With the successive improvements in these data, analyses will be possible that build upon the present study to resolve the interannual variability in the energy budget and to quantify, more precisely, its role in a changing climate. This study thus offers an advance while also providing an improved estimate of the energy budget that can be used to evaluate the quality of present-day model simulations.

*Acknowledgments.* This research is partially sponsored by the NOAA CLIVAR and CCDD programs under Grant NA07OAR4310051. The CERES data were obtained from the NASA Langley Distributed Data Archive. We thank Bruce Wielicki and other members of the CERES team for their thoughtful comments and discussions. Electronic versions of the yearly and pentadal heat content fields used here and data distribution maps by yearly and pentadal compositing periods are available online (http://www.nodc.noaa.gov/OC5/indprod.html).

## REFERENCES

AchutaRao, K. M., B. D. Santer, P. J. Gleckler, K. E. Taylor, D. W. Pierce, T. P. Barnett, and T. M. L. Wigley, 2006: Variability of ocean heat uptake: Reconciling observations and models. *J. Geophys. Res.,* **111,** C05019, doi:10.1029/2005JC003136.

Behringer, D. W., 2007: The Global Ocean Data Assimilation System (GODAS) at NCEP. Preprints, *11th Symp. on Integrated Observing and Assimilation Systems for the Atmosphere, Oceans, and Land Surface* (*IOAS-AOLS*), San Antonio, TX,

Amer. Meteor. Soc., 3.3. [Available online at http://ams.confex.com/ams/pdfpapers/119541.pdf.]

Bonan, G. B., K. W. Oleson, M. Vertenstein, S. Levis, X. B. Zeng, Y. J. Dai, R. E. Dickinson, and Z. L. Yang, 2002: The land surface climatology of the Community Land Model coupled to the NCAR Community Climate Model. *J. Climate,* **15,** 3123–3149.

Czaja, A., and J. Marshall, 2006: The partitioning of poleward heat transport between the atmosphere and ocean. *J. Atmos. Sci.,* **63,** 1498–1511.

Dickinson, R. E., K. W. Oleson, G. B. Bonan, F. Hoffman, P. Thornton, M. Vertenstein, Z.-L. Yang, and X. Zeng, 2006: The Community Land Model and its climate statistics as a component of the Community Climate System Model. *J. Climate,* **19,** 2302–2324.

Fasullo, J. T., and K. E. Trenberth, 2008: The annual cycle of the energy budget. Part I: Global mean and land–ocean exchanges, *J. Climate,* **21,** 2297–2313.

Gouretski, V., and K. P. Koltermann, 2007: How much is the ocean really warming? *Geophys. Res. Lett.,* **34,** L01610, doi:10.1029/2006GL027834.

Hansen, J., and Coauthors, 2005: Earth's energy imbalance: Confirmation and implications. *Science,* **308,** 1431–1435.

Held, I. M., 2001: The partitioning of the poleward energy transport between the tropical ocean and atmosphere. *J. Atmos. Sci.,* **58,** 943–948.

Huang, S., 2006: Land warming as part of global warming. *Eos, Trans. Amer. Geophys. Union,* **87,** 477, 780.

Ishii, M., M. Kimoto, K. Sakamoto, and S. I. Iwasaki, 2006: Steric sea level changes estimated from historical ocean subsurface temperature and salinity analyses. *J. Oceanogr.,* **62,** 155–170.

Kalnay, E., and Coauthors, 1996: The NCEP/NCAR 40-Year Reanalysis Project. *Bull. Amer. Meteor. Soc.,* **77,** 437–471.

Kistler, R., and Coauthors, 2001: The NCEP–NCAR 50-Year Reanalysis: Monthly means CD-ROM and documentation. *Bull. Amer. Meteor. Soc.,* **82,** 247–267.

Levitus, S., J. Antonov, and T. Boyer, 2005: Warming of the world ocean, 1955–2003. *Geophys. Res. Lett.,* **32,** L02604, doi:10.1029/2004GL021592.

Locarnini, R. A., A. V. Mishonov, J. I. Antonov, T. P. Boyer, and H. E. Garcia, 2006. *Temperature.* Vol. 1, *World Ocean Atlas 2005,* NOAA Atlas NESDIS 61, 182 pp.

Lombard, A., and Coauthors, 2007: Estimation of steric sea level variations from combined GRACE and *Jason-1* data. *Earth Planet. Sci. Lett.,* **254,** 192–202.

Oort, A. H., and T. H. Vonder Haar, 1976: On the observed annual cycle in the ocean–atmosphere heat balance over the Northern Hemisphere. *J. Phys. Oceanogr.,* **6,** 781–800.

Qian, T., A. Dai, K. E. Trenberth, and K. W. Oleson, 2006: Simulation of global land surface conditions from 1948 to 2004. Part I: Forcing data and evaluation. *J. Hydrometeor.,* **7,** 953–975.

Serreze, M. C., A. P. Barrett, A. J. Slater, M. Steele, J. Zhang, and K. E. Trenberth, 2007: The large-scale energy budget of the Arctic. *J. Geophys. Res.,* **112,** D11122, doi:10.1029/2006JD008230.

Trenberth, K. E., 1997: Using atmospheric budgets as a constraint on surface fluxes. *J. Climate,* **10,** 2796–2809.

——, and A. Solomon, 1994: The global heat balance: Heat transports in the atmosphere and ocean. *Climate Dyn.,* **10,** 107–134.

——, and C. J. Guillemot, 1998: Evaluation of the atmospheric moisture and hydrological cycle in the NCEP/NCAR reanalyses. *Climate Dyn.,* **14,** 213–231.

——, and J. M. Caron, 2001: Estimates of meridional atmosphere and ocean heat transports. *J. Climate,* **14,** 3433–3443.

——, and D. P. Stepaniak, 2003a: Covariability of components of poleward atmospheric energy transports on seasonal and interannual timescales. *J. Climate,* **16,** 3690–3704.

——, and ——, 2003b: Seamless poleward atmospheric energy transports and implications for the Hadley circulation. *J. Climate,* **16,** 3705–3721.

——, and ——, 2004: The flow of energy through the Earth's climate system. *Quart. J. Roy. Meteor. Soc.,* **130,** 2677–2701.

——, J. M. Caron, and D. P. Stepaniak, 2001: The atmospheric energy budget and implications for surface fluxes and ocean heat transports. *Climate Dyn.,* **17,** 259–276.

——, D. P. Stepaniak, and J. M. Caron, 2002: Accuracy of atmospheric energy budgets from analyses. *J. Climate,* **15,** 3343–3360.

——, J. Fasullo, and L. Smith, 2005: Trends and variability in column-integrated water vapor. *Climate Dyn.,* **24,** 741–758.

——, L. Smith, T. Qian, A. Dai, and J. Fasullo, 2007: Estimates of the global water budget and its annual cycle using observational and model data. *J. Hydrometeor.,* **8,** 758–769.

Uppala, S. M., and Coauthors, 2005: The ERA-40 reanalysis. *Quart. J. Roy. Meteor. Soc.,* **131,** 2961–3012.

Wielicki, B. A., K. Priestley, P. Minnis, N. Loeb, D. Kratz, T. Charlock, D. Doelling, and D. Young, 2006: CERES radiation budget accuracy overview. Preprints, *12th Conf. on Atmospheric Radiation,* Madison, WI, Amer. Meteor. Soc., 9.1. [Available online at http://ams.confex.com/ams/Madison2006/techprogram/paper_112371.htm.]

Willis, J. K., D. Roemmich, and B. Cornuelle, 2004: Interannual variability in upper-ocean heat content, temperature and thermosteric expansion on global scales. *J. Geophys. Res.,* **109,** C12036, doi:10.1029/2003JC002260c.

Wunsch, C., 2005: The total meridional heat flux and its oceanic and atmospheric partition. *J. Climate,* **18,** 4374–4380.

Zhang, Y.-C., and W. B. Rossow, 1997: Estimating meridional energy transports by the atmospheric and oceanic general circulations using boundary fluxes. *J. Climate,* **10,** 2358–2373.